applied sciences

MDPI

Article

Optimizing Cotton Picker Cab Layout Based on Upper-Limb Biomechanics Using the AMS-RF-DBO Framework

Haocheng Tang [1,2], Zikai Wei [1,2,3,*], Yongman Zhao [1,2,*], Yating Li [1,2], Zhongbiao He [1,2], Jingqi Gong [1,2] and Yuan Wu [1,2]

[1] College of Mechanical and Electrical Engineering, Shihezi University, Shihezi 832003, China; tanghaocheng@xjshzu.com (H.T.); liyating98@xjshzu.com (Y.L.); hezhongbiao@xjshzu.com (Z.H.); gongjingqi@xjshzu.com (J.G.); wuyuan1@xjshzu.com (Y.W.)
[2] Key Laboratory of Northwest Agricultural Equipment, Ministry of Agriculture and Rural Affairs, Shihezi 832003, China
[3] Department of Industrial Engineering, Tsinghua University, Beijing 100084, China
* Correspondence: zkwei@shzu.edu.cn (Z.W.); zhrym@shzu.edu.cn (Y.Z.)

Abstract

Prolonged operation of cotton picker poses significant risks of work-related musculoskeletal disorders (WMSDs), primarily driven by non-ergonomic cab layouts that fail to accommodate the unique "left-hand steering, right-hand lever" operational mode. Traditional optimization methods, relying on general digital human models or isolated surface electromyography (sEMG) measurements, often lack the physiological fidelity and computational efficiency for high-dimensional, personalized design. To address this interdisciplinary challenge in agricultural engineering and ergonomics, this study proposes a novel AMS-RF-DBO framework that integrates high-fidelity biomechanical simulation with intelligent optimization. A driver–cabin biomechanical model was developed using the AnyBody Modeling System (AMS) and validated against sEMG data (ICC = 0.695). This model generated a dataset linking cab layout parameters to maximum muscle activation (MA). Using steering wheel and control lever coordinates (X, Y, Z) as inputs, a Random Forest (RF) regression model demonstrated strong performance (R^2 = 0.91). Optimization with the Dung Beetle Optimizer (DBO) algorithm yielded an optimal configuration: steering wheel (L1 = 434 mm, H1 = 738 mm, θ = 32°) and control lever (L2 = 357 mm, H2 = 782 mm, M = 411 mm), reducing upper-limb MA from 3.82% to 1.47% and peak muscle load by 61.5%. This study not only provides empirical support for ergonomic cab design in cotton pickers to reduce operator fatigue and health risks but also establishes a replicable technical paradigm for ergonomic optimization of other specialized agricultural machinery.

Keywords: cotton picker cab; upper limb biomechanics; RF-DBO; muscle activation; ergonomic optimization

Check for updates

Academic Editor: Arkady Voloshin

Received: 5 November 2025
Revised: 13 December 2025
Accepted: 20 December 2025
Published: 30 December 2025

Copyright: © 2025 by the authors. Licensee MDPI, Basel, Switzerland. This article is an open access article distributed under the terms and conditions of the Creative Commons Attribution (CC BY) license.

1. Introduction

Xinjiang accounts for over 92% of China's cotton output, and its >90% mechanical harvesting rate is a core indicator of the transition to precision agriculture [1–3]. However, behind the efficient development of agricultural mechanization lies a significant risk posed by a pressing occupational health concern that cannot be overlooked.

Globally, agricultural workers are consistently exposed to high risks of occupational diseases and injuries [4], with cotton harvesting operations in Xinjiang being a particularly notable example. Drivers work 12–14 h daily, and prolonged, high-intensity operation

patterns easily lead to work-related musculoskeletal disorders (WMSDs), which worsen with continuous work [5–8]. WMSDs not only cause personal suffering but can also impair operational performance, ultimately undermining the sustainability of the cotton harvesting sector. This conflict between the demands of mechanized work and the well-being of operators has become a critical challenge in ensuring the sustainable development of cotton harvesting, a key area in agricultural engineering.

1.1. Operational Characteristics and Ergonomic Challenges of Cotton Pickers

The cab control layout is the key human–machine interface for cotton pickers, as the arrangement of control devices directly determines the mechanical strain on the driver's musculoskeletal system [9]. Compared to traditional agricultural machinery, cotton pickers have a unique operational mode, where the "left hand continuously controls the steering wheel, while the right hand operates the control lever". This asymmetrical operational pattern places uneven, sustained loads on the upper-limb musculature, leading to potential musculoskeletal strain. More importantly, domestic cotton pickers lack specialized design standards for their cabs, resulting in mismatched layouts that exacerbate ergonomic issues. This mismatch in operational modes and standards highlight a critical challenge in agricultural ergonomics: how to optimize cab layouts for specialized cotton pickers to protect operator health.

The operational mode of a cotton picker differs from that of traditional agricultural machinery [10]. For example, tractors typically use a "hand–foot coordination with intermittent operation" mode [11], while excavators operate with "multiple alternating movements [12]". In contrast, the cotton picker requires "single upper-limb repetitive motion with coordination between both upper limbs", which necessitates prolonged use of the upper body. As a result, existing evaluation systems for traditional agricultural machinery are inadequate for cotton pickers. The lack of research on this unique operational mode makes current cab design standards and ergonomic theories insufficient to address these issues.

Additionally, domestic cotton picker cabs lack unified design standards and differ significantly from the standards used for tractors and other traditional agricultural machinery. This discrepancy results in poor comfort levels for operators, who experience discomfort during prolonged operation. Imported cotton pickers often follow European ergonomic standards, which fail to account for the differences in height, arm length, and seating posture among Chinese operators. This "standard mismatch" not only affects operator comfort but also increases the risk of WMSDs, becoming a key challenge in the mechanization of cotton picking.

Therefore, optimizing the control layout of cotton picker cabs, especially the rational arrangement of control devices, is crucial for reducing the risk of WMSDs and enhancing operational comfort.

1.2. Current Cab Optimization Approaches

1.2.1. Simulation-Based Methods

In recent years, numerous scholars have explored the optimization of agricultural and engineering machinery cabins, primarily focusing on simulation modeling and established comfort evaluation metrics. However, overreliance on predefined simulation tools makes it difficult to accurately calculate biomechanical indicators such as muscle load and joint stress, presenting certain limitations. Most current studies rely on general simulation tools such as JACK v8.0, Creo Manikin v12.0.0.0, RAMSIS V5R20, SAMMIE v8.5, or finite element analysis software. For example, Wu et al. [13] used JACK to establish a tractor model for ergonomic evaluation of the human–machine interface; Wang et al. [14] proposed

improvement schemes for excavator–loader cabs based on the same software; Xu et al. [15] optimized equipment layout by analyzing operational reachability through JACK; Qu et al. [16] developed a quantitative evaluation system for work posture comfort based on Creo secondary development and musculoskeletal mechanics analysis, providing a quantitative and efficient solution for optimizing the human-machine layout of workover rigs; Cheng et al. [17] optimized the comfort of engineering machinery seats via Hypermesh; and Rathod and colleagues employed RAMSIS to optimize the ergonomics of a commercial truck cab [18].

While valuable for preliminary assessments, these tools and methods often rely on simplified kinematic human models and preset human body parameters for comfort evaluation. This makes it difficult to reflect individual differences among drivers, limiting the practical adaptability of optimization results. Moreover, these methods struggle to accurately quantify the internal physiological loads, such as individual muscle forces and joint stresses, which are the direct causes of fatigue and WMSDs. Consequently, they offer limited capability for predictive, physiology-based optimization and fail to adequately address the sustained, asymmetric muscle activation (MA) patterns inherent in specialized operations like cotton harvesting.

1.2.2. Biomechanical Evaluation Methods

To overcome these limitations of general simulation, biomechanical evaluation methods have become a growing area of research due to their ability to provide quantitative, precise assessments of comfort and health risks [19]. These methods focus on linking ergonomic comfort directly with biomechanical characteristics, offering a more detailed understanding of operator well-being [20]. For instance, LECOCQ et al. [21] compared the effects of different seats on neuromuscular fatigue during driving, while Chi et al. [22] optimized operational interfaces by considering the interaction between hand width and keyboard size. Xin et al. [23] analyzed upper-limb fatigue patterns in excavator drivers by collecting surface electromyography (sEMG) signals, thereby optimizing cab layout design.

However, biomechanical methods also faces certain limitations. On one hand, relying solely on sEMG for fatigue evaluation has constraints in data timeliness, on-site operability, and signal processing complexity. On the other hand, existing biomechanical research has predominantly focused on traditional agricultural machinery, such as tractors, and does not address the unique needs of cotton pickers. The operational modes of cotton pickers differ significantly from those of traditional machinery, complicating the direct application of existing evaluation systems. Additionally, the lack of research on cab optimization for this specific type of equipment further exacerbates the issue, as current ergonomic models are inadequate. This gap is further compounded by the lack of tailored cab design standards for domestic models and anthropometric mismatches in imported ones.

Therefore, there is a critical need for a dedicated optimization framework that integrates high-fidelity biomechanical simulation with intelligent optimization, capable of addressing the specific physiological loads and operational patterns of cotton picker operators.

1.3. The Proposed AMS-RF-DBO Framework

To address the above interdisciplinary challenges, this study proposes a novel AMS-RF-DBO framework that integrates high-fidelity biomechanical simulation with intelligent optimization. At the biomechanical simulation level, the AnyBody Modeling System (AMS) is employed to replace traditional tools and single sEMG testing. AMS possesses high-precision musculoskeletal modeling and powerful inverse dynamics analysis capabilities [24], outperforming general simulation software in model processing, simulation

analysis, and data output, while avoiding the timeliness and complexity limitations of sEMG. Its successful application in vehicle ergonomics has been previously validated. Xu et al. [25] utilized AMS to establish a driver model and optimized tractor seat parameters to minimize muscle force and joint stress. Zhang et al. [26] constructed a "driver–operation action–working environment" coupling model to quantitatively analyze lower-limb fatigue accumulation patterns. Similarly, Xu et al. [27] determined the optimal steering wheel position based on AMS to reduce upper-limb muscle load. In terms of optimization algorithms, the Dung Beetle Optimizer (DBO) is introduced to address the shortcomings of traditional methods (such as response surface methodology [28]), which heavily rely on experimental design and are prone to falling into local optima in high-dimensional nonlinear problems. DBO simulates the intelligent behaviors of dung beetles in nature, including ball rolling, dancing, and foraging, thereby achieving an efficient balance between global exploration and local development, effectively avoiding premature convergence. DBO is particularly suitable for complex optimization problems with multiple parameters and nonlinearity, such as cab layout design [29]. Compared with other intelligent algorithms, such as hybrid particle swarm optimization–genetic algorithm (PSO-GA) [30] and neural network models [31], DBO exhibits superior adaptability in multi-objective collaborative optimization and better aligns with the multidimensional requirements of cab layout configuration. The synergy between the high-fidelity AMS biomechanical simulation and the robust global search capability of the DBO algorithm forms the core of our proposed framework. The AMS-RF-DBO approach not only offers a tailored solution for optimizing cotton picker cabs but also presents a transferable methodology applicable to the ergonomic design of other types of specialized machinery

Therefore, to address the ergonomic challenges arising from the unique operation in cotton pickers, this study establishes an integrated framework aimed at significantly reducing upper-limb muscle load, thereby mitigating fatigue and WMSDs. Taking the cab of the 4MZD-6 cotton picker as a case study, the specific objectives of this study are as follows:

(1) To develop a biomechanical driver–cabin coupling model using the AMS and validate its accuracy against sEMG data, establishing a reliable simulation basis for muscle load assessment.
(2) To construct an RF regression model that predicts maximum MA based on cab layout parameters and to employ the DBO algorithm to identify an optimal configuration that minimizes upper-limb muscle effort.
(3) To propose and verify a reusable AMS-RF-DBO technical framework that provides a replicable paradigm for the ergonomic design of other specialized agricultural machinery, ultimately promoting operator well-being.

2. Materials and Methods

2.1. Biomechanical Modeling and Simulation

2.1.1. Musculoskeletal Model

The AMS and its associated model library from Aalborg University were selected for their high-fidelity musculoskeletal modeling capabilities and validated inverse dynamics solvers, which are essential for calculating individual muscle forces and activations [32]. Therefore, this study employs a human musculoskeletal model library developed by Aalborg University in Denmark (Figure 1). Since the original model is based on Western anthropometric data, which differs from the anthropometric characteristics of the Chinese population, this study utilized geometric scaling methods to adjust the dimensions of the original human model [33]. Specifically, a linear scaling approach was applied based on the standard geometric scaling functionality within the AMS. The scaling was performed

segment-by-segment using the length references derived from the 50th percentile Chinese adult male dimensions (GB/T 10000-2023 [34]). Key scaling factors were calculated for major body segments based on the ratio of the target anthropometric lengths (e.g., sitting shoulder height, and upper arm length) to the corresponding default lengths in the Aalborg University model. This ensured that the overall proportions of the scaled model accurately represented the target population.

The model scaling parameters were determined based on the 50th percentile human body size data from the "Chinese Adult Human Body Dimensions" (GB/T 10000-2023) standard. The issue of muscle force distribution—an inherent challenge in the inverse kinematics simulation of this redundant musculoskeletal system—is resolved through the default "minimum/maximum" polynomial order optimization criterion in the AMS software (version 7.4). This optimization criterion effectively minimizes the sum of cubes of muscle stresses across all muscles [32]. We employ bilateral symmetrical scaling of the upper limbs, assuming that the upper limbs possess bilaterally symmetrical anthropometric characteristics.

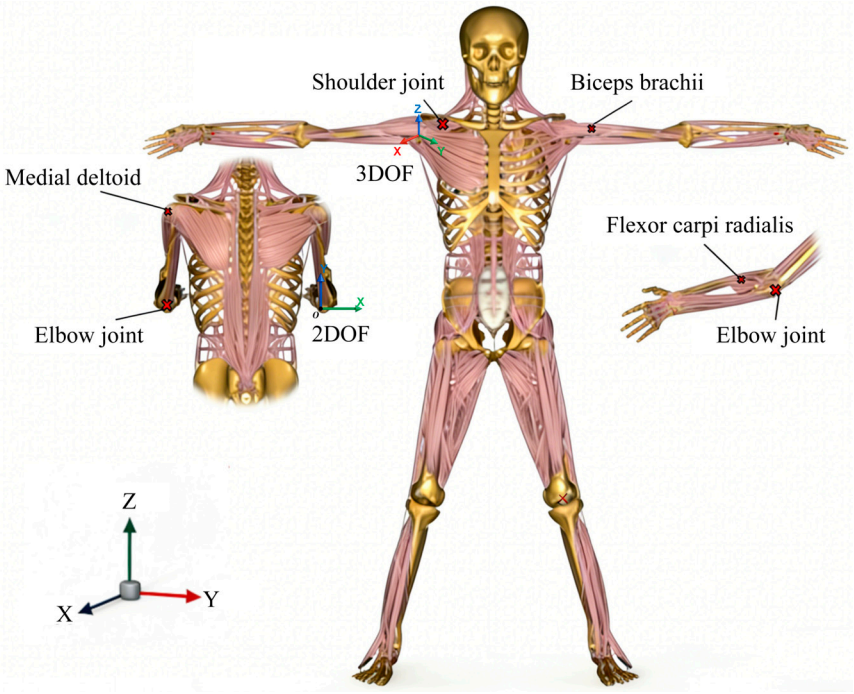


Figure 1. Human musculoskeletal model.

2.1.2. Cab Modeling and Driver–Cabin Coupling

The cab model primarily consists of an adjustable seat, an adjustable steering wheel, and adjustable control devices. A three-dimensional model of the cab was created using SolidWorks software v2023, with all dimensions based on actual measurement data, as shown in Figure 2. After modeling, the cab model was saved as an STL file and exported in encoded form. The system units were set to millimeters (mm), and the part coordinate system was defaulted to the internal model coordinate system. The model was then imported into the AMS software environment. Six rigid bodies were created using the "AnySeg" class, corresponding to the seat, steering wheel, steering wheel base, right-hand control panel, joystick, and joystick base. To ensure the structural integrity of the system, coupling constraints were set. Specifically, the rigid bodies within the driver's cabin model were constrained and connected. The specific coordinate parameters of each coupling point are detailed in Table 1 to ensure precise alignment between model components and the rationality of motion constraints. After importing all components, the coordinate

system of the human musculoskeletal model was rigidly connected to the world coordinate system, and the base of the upper-limb fitness device was rigidly connected to the world coordinate system. Different connection commands were used to select the appropriate type of kinematic pair between cooperating parts by connecting the origins of their local coordinate systems and specifying the axis direction for relative motion between them. Finally, the biomechanical coupling model of the cotton picker cab was established, as shown in Figure 3.

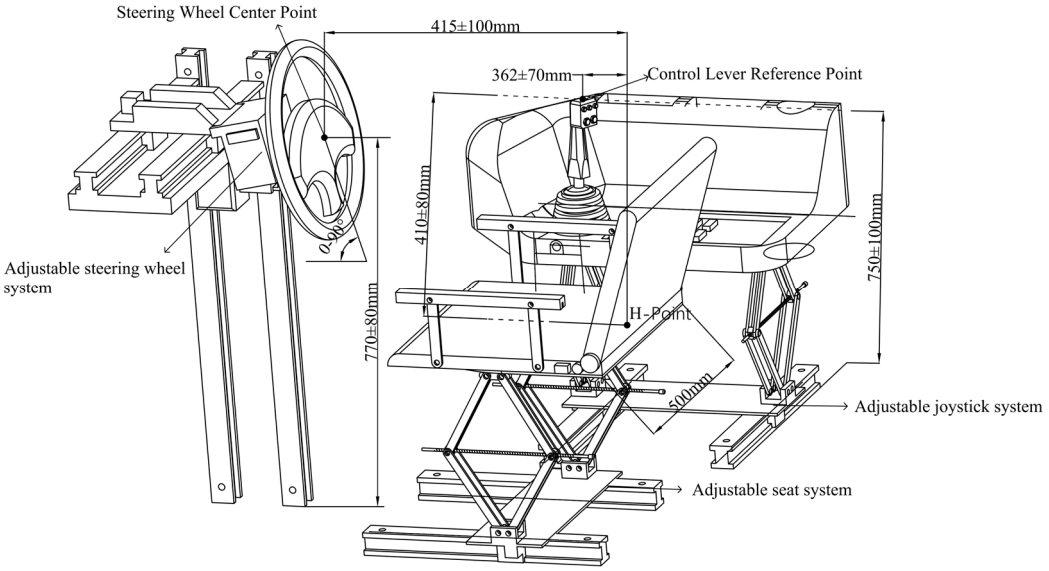


Figure 2. Cab model.

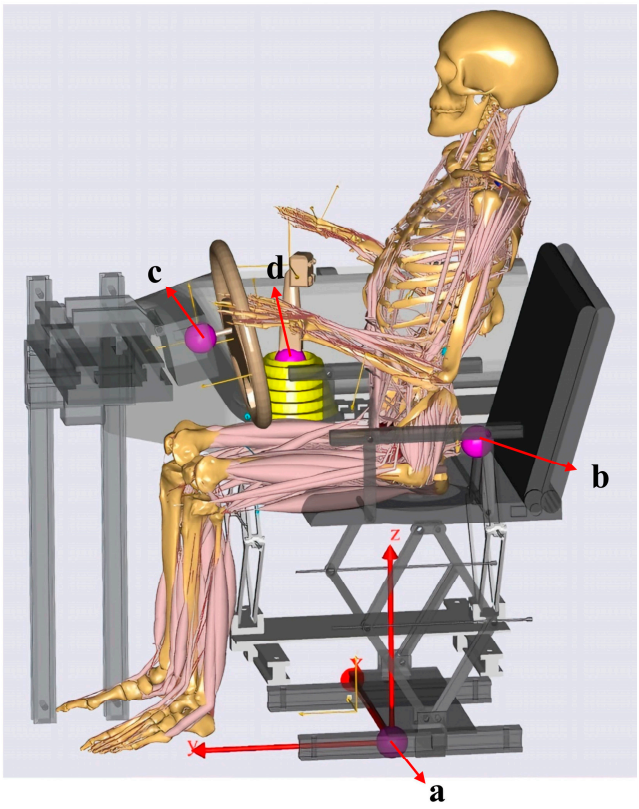


Figure 3. Biomechanical human–machine coupling model.

Table 1. Coordinate parameters of coupling points in the AnyBody human–machine coupling system.

Coupling Point Name	X	Y	Z	Parent Segment	Child Segment	Clarification
connect_to_global (a)	0.045	−0.17	0.55	Geodetic	Seating	Connection to the geodetic coordinate system
connect_to_wheel (c)	−0.08	0.36	0.80	Steering wheel base	Steering wheel	Fixed steering wheel
connect_to_handle (d)	0.01	0.01	0.01	Joystick base	Control stick	Fixed rocker
pelvis_seats (b)	0	0	0	Seating	Pelvic	Anchor

2.2. Experiment Design

2.2.1. Independent Variables

As shown in Table 2, the position parameters of the steering wheel and control lever were selected as independent variables. Figure 4 shows a schematic diagram of each human–machine layout factor. According to the general national standards for the layout of agricultural machinery cabs, five levels were set for each factor, as shown in Table 3.

Table 2. Human–machine arrangement factors.

Steering Wheel Position Parameters	Control Lever Position Parameters
Distance from steering wheel center to the H-point L1 (mm)	Distance from control lever center to the H-point L2 (mm)
Height of steering wheel center from ground H1 (mm)	Height of control lever from ground H2 (mm)
Angle between steering wheel and horizontal plane θ (°)	Horizontal distance from control lever center to H-point M (mm)

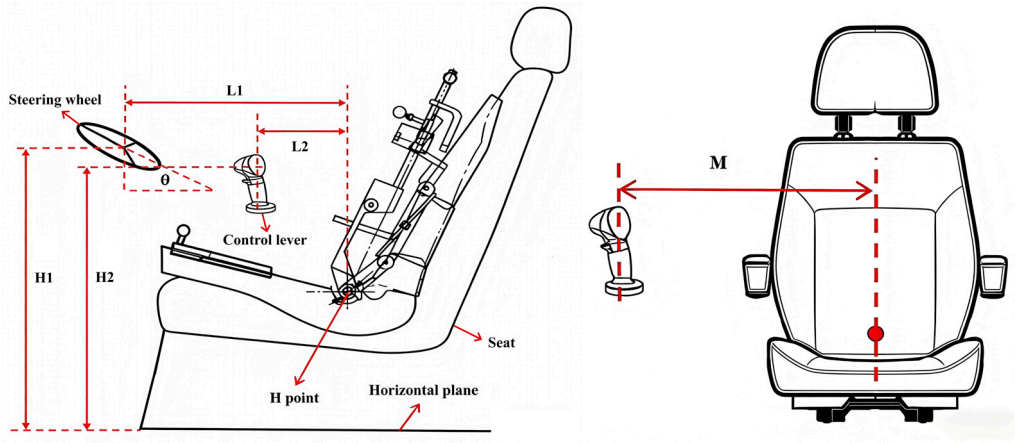


Figure 4. Schematic diagram of the cab layout parameters: (**a**) steering wheel; (**b**) control lever.

Table 3. Human–machine layout factor levels.

Factor	Level 1	Level 2	Level 3	Level 4	Level 5
L1 (mm)	400	425	450	475	500
θ (°)	0	10	20	30	40
H1 (mm)	720	745	770	795	820
L2 (mm)	300	320	340	360	380
H2 (mm)	710	735	760	785	810
M (mm)	375	400	425	450	475

2.2.2. Participants

The survey found that cotton picker operators are predominantly male. Therefore, this study recruited 10 healthy male participants who met the 50th percentile physical fitness standards (age 27 ± 2.6 years, height 172 ± 3.0 cm, weight 69 ± 3.4 kg, coefficient of

variation (CV) < 10%). All participants had driving experience and reported no upper-limb musculoskeletal disorders. To ensure stable muscle condition, participants were instructed to refrain from strenuous physical activity 24 h prior to the experiment and underwent pre-experimental training. Informed consent was obtained from all participants. After the experiment, all participants received a participant fee of CNY 150. The mean values of the primary physical measurement data for the experimental participant group are summarized in Table 4.

Table 4. Average anthropometric measurements of the participant group (n = 10).

Seated Shoulder Height (mm)	Shoulder Width (mm)	Seated Elbow Height (mm)	Hand Length (mm)	Upper Arm Length (mm)	Forearm Length (mm)	Hand Width (mm)
1455	630	275	180	332	240	95

2.2.3. Experimental Setup and Apparatus

As shown in Figure 5, the cotton picker cab simulation experiment platform was constructed based on the actual layout of a cotton picker cab. It was equipped with a steering wheel adjustable in height from the ground (H1: 700–900 mm), front-to-back distance from the H-point (L1: 375–575 mm), and steering wheel tilt angle (θ: 0–90°). Similarly, the control lever was adjustable in front-to-back distance from the H-point (L2: 300–400 mm), lateral distance from the H-point (M: 350–500 mm), and height from the ground (H2: 650–850 mm).

The steering wheel torque was set to 2 N·m, a value determined based on actual cotton picker torque standards and measured using a WZX-I type (±0.1 N·m) steering parameter tester. The steering wheel tilt angle was adjusted using a DI-503A type digital tilt angle meter. sEMG data were collected with the Beijing Hengzhi Technology Eve sEMG multi-channel physiological data acquisition system, which uses medical-grade Ag/AgCl surface electrodes (diameter 10 mm, spacing 20 mm) and positions target muscle movement points according to SENIAM standards. The system integrates a digital signal processing module, supporting real-time bandpass filtering (20–500 Hz), 50 Hz power frequency notch filtering, and root mean square (RMS) value calculation functions.

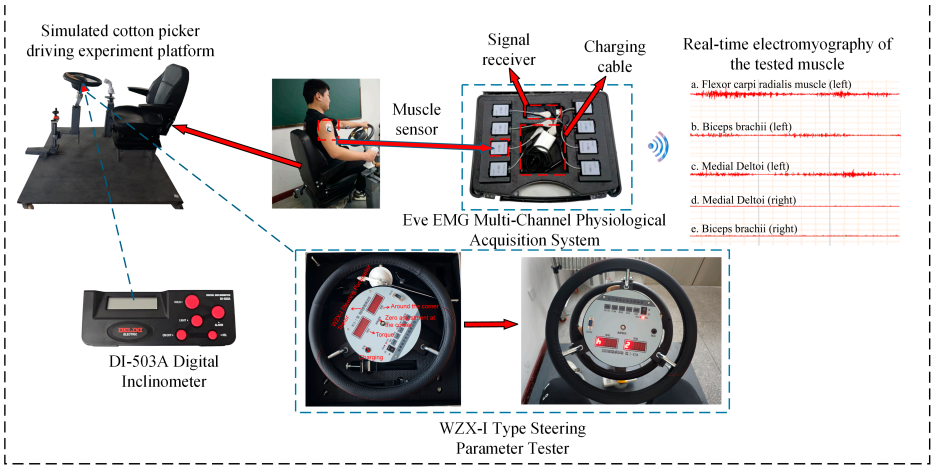


Figure 5. Experimental equipment.

2.2.4. Maximum Voluntary Contraction (MVC) Calibration

Before formal testing, upper-limb muscle MVC calibration was performed in accordance with the standard procedures of the International Society of Biomechanics. The specific operational process was as follows:

(1) The surface skin of the target muscle group was repeatedly wiped with 70% medical alcohol cotton balls to remove epidermal oils and the stratum corneum.
(2) Electrodes were positioned according to the SENIAM guidelines.

This preprocessing procedure effectively reduces skin–electrode interface impedance and significantly improves the signal-to-noise ratio [35,36]. Since surface muscles are easily accessible, provide stable signal acquisition, and represent overall muscle activity [37], they are ideal subjects for study. Based on electromyographic signal characteristics, muscles with higher recruitment of motor units and significant changes in activation patterns during tasks were selected from both sides of the upper-limb muscle groups. These muscles were chosen to accurately reflect the muscle load characteristics of drivers under specific operational conditions. During driving, the arm muscles include the biceps brachii for stabilizing the handle, the middle head of the deltoid muscle and the lateral head of the triceps brachii for extending the handle, and the radial wrist flexor for wrist flexion and stabilization. Therefore, the biceps brachii, middle deltoid, lateral head of the triceps brachii, and flexor carpi radialis were selected as target muscles, as shown in Figure 6. According to the International Society of Electrophysiology and Kinesiology (ISEK) [38] guidelines, MVC calibration (Figure 7) was performed using the method of taking the maximum value from three repeated measurements. Each contraction lasted 10 s, with a 5 min rest interval between trials to avoid contraction force decay caused by muscle fatigue. The specific calibration postures for each muscle were as follows:

(1) Biceps brachii: Electrodes were placed on the proximal one-third of the elbow crease, with the subject flexing the elbow to 90° against desk resistance.
(2) Middle deltoid: The "empty can" position [39] (shoulder abduction 90° with internal rotation) was used, and electrodes were placed along the line connecting the acromion and lateral epicondyle;
(3) Triceps brachii: Electrodes were placed two finger-widths lateral to the line connecting the posterior acromion and olecranon process. The subject flexed the elbow to 90° and pushed against a wall.
(4) Flexor carpi radialis: Electrodes were placed along the longitudinal axis of the muscle belly. The subject raised their four fingers against resistance on the table. All electrodes were spaced 20 mm apart, and calibration was performed simultaneously on both sides.

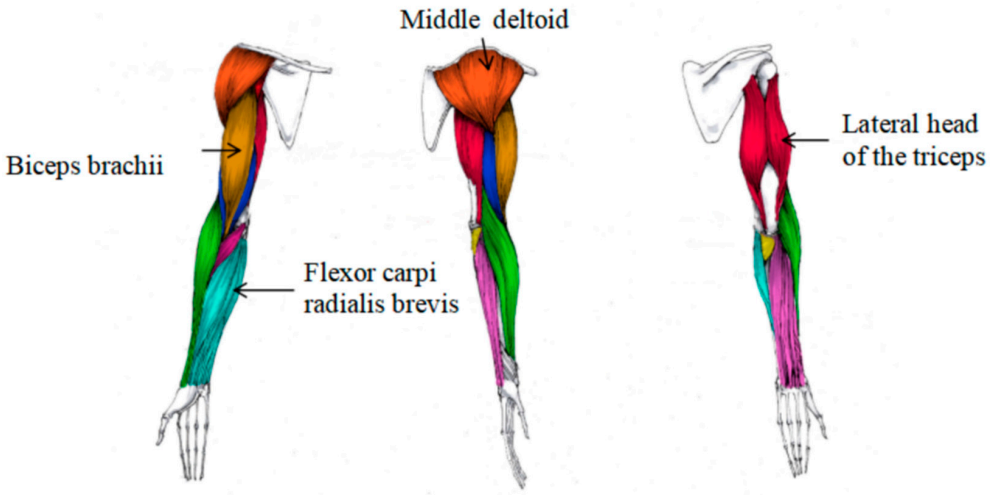


Figure 6. Schematic diagram of upper-limb muscles.

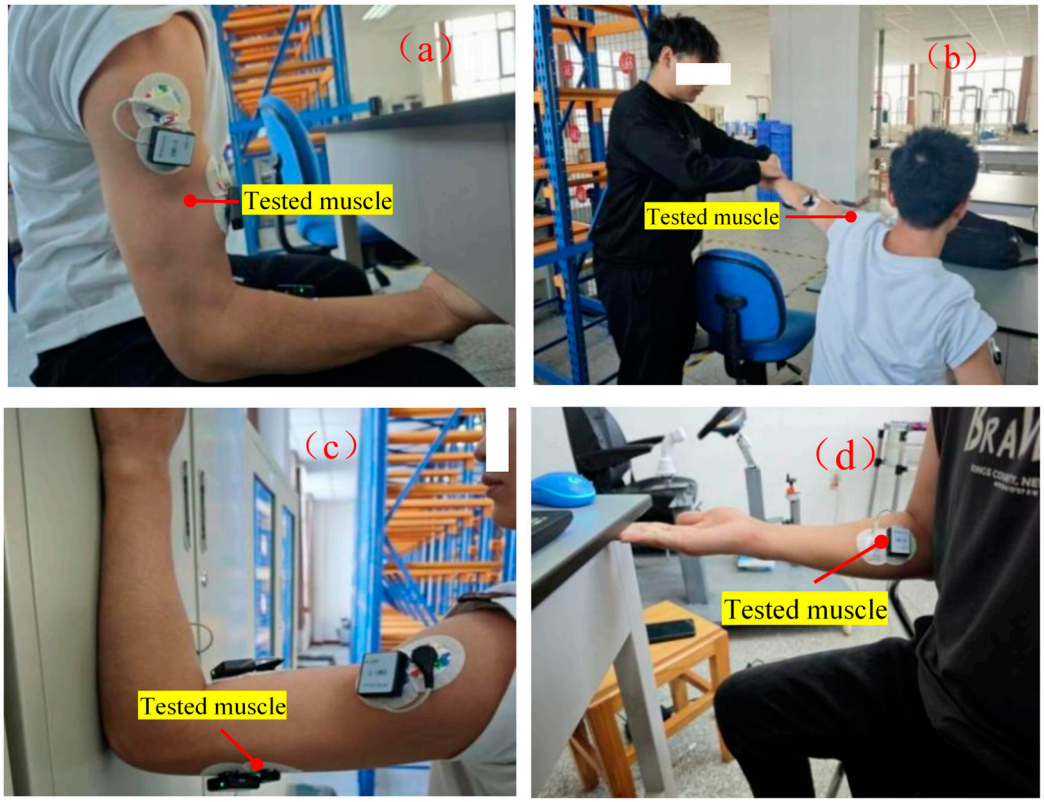


Figure 7. MVC calibration postures: (**a**) biceps brachii; (**b**) middle deltoid; (**c**) lateral head of triceps; (**d**) flexor carpi radialis.

2.3. sEMG Signal Processing and MA Calculation

Studies on the effective frequency range of sEMG signals indicate that signal energy is primarily distributed between 10 and 500 Hz, with the upper limit of effective information ranging from 400 to 500 Hz and the lower limit from 10 to 20 Hz. Given that raw sEMG signals are susceptible to environmental noise and individual variability, this study employed the electromyographic signal preprocessing module of the Eve sEMG multi-channel physiological data acquisition system to enhance signal quality. The standardized workflow comprises the following steps [40]: (1) Initial signal processing using a third-order Butterworth bandpass filter with a cutoff frequency range of 10–480 Hz. This parameter configuration effectively preserves the physiologically relevant frequency components of sEMG signals (with primary energy concentrated between 20 and 450 Hz) while eliminating low-frequency baseline drift (below 10 Hz) and high-frequency noise interference (above 480 Hz). Secondary processing employs a second-order Butterworth low-pass filter with identical cutoff frequencies (10–480 Hz). This step further optimizes signal quality, elevating the signal-to-noise ratio (SNR) to over 25 dB while ensuring signal distortion remains below 3%. (2) The root mean square (RMS) value is then calculated over a moving window (window length: 3 s). (3) This RMS value is subsequently divided by the average RMS of three maximum voluntary contractions of the same muscle to obtain the normalized muscle activation (MA). All filtering processes utilize the cumulative discharge of action potentials from zero-phase motor units as an effective parameter for evaluating MA levels and contraction intensity. The calculation formula is shown in Equation (1):

$$iEMG = \int_0^T |EMG(t)|dt \quad (1)$$

where T represents the time window length, which indicates the electromyographic potential value. The RMS value can be used to represent MA levels, calculated as shown in Equation (2):

$$RMS = \sqrt{\frac{1}{T}\int_0^T EMG(t)^2 dt} \quad (2)$$

The normalized ratio of the RMS value obtained from the test bench experiment to the root mean square value of electromyography (RMS_{MVC}) measured under MVC conditions can quantitatively characterize the maximum MA. RMS_{MVC} is the average value of three MVCs. The calculation formula for this indicator is shown in Equation (3):

$$MA = \frac{RMS}{RMS_{MVC}} \times 100\% \quad (3)$$

The iterative ANOVA method was applied to the processed data until the p-value of the largest residual across all groups exceeded 0.05, which led to the removal of 2.7% of outlying observations.

2.4. Experimental Procedure

Prior to the experiment, all participants signed informed consent forms and underwent MVC calibration. After calibration, the acquisition of sEMG signals began. The driving posture for the formal experiment was as follows: The left hand was placed at the midpoint of the left half of the steering wheel. From this position, the left hand performed a series of rotational movements: a 90° clockwise rotation, followed by a 180° counterclockwise rotation, and finishing with another 90° clockwise rotation. Each complete movement cycle lasted 3 s, and each participant performed the test three times. After each test, the RMS value of the measured sEMG signals was calculated, and the average of the three tests across 10 participants was used as the final value. An electronic metronome (KORG KDM-2, accuracy $\pm$ 0.1%) was used to maintain a constant rhythm of 60 bpm. Real-time auditory feedback was provided to ensure that all participants maintained a consistent rotation frequency and continuous motion throughout the task. At the same time, the right hand remained in a static posture, continuously gripping the control handle. A 5 min inter-session interval was maintained between each experiment. This allowed participants' muscle states to return to baseline levels, minimizing errors caused by reduced muscle coordination due to accumulated fatigue [41].

2.5. AMS-RF-DBO Prediction and Optimization Framework

To quantify the relationship between human–machine interaction position parameters and muscle load, a biomechanical prediction model was constructed using Random Forest (RF) regression. Figure 8 illustrates a schematic diagram of the AMS-RF-DBO framework. Human–machine interaction parameters from the cotton picker cab (including L1, H1, θ, L2, H2, and M) served as input feature vectors, while the MA level measured by the biomechanical model was the sole output of the prediction model. The dataset was partitioned using three-fold cross-validation for model training.

To address the issue of low-upper-limb MA, the DBO algorithm was employed for optimization (Figure 9). This algorithm was proposed by Xue and Shen in 2022. The DBO algorithm employs biomimetic design principles, translating the dung beetle's rolling, dancing, egg-laying, foraging, and scavenging behaviors into optimization operators. Their calculation formulas are shown in Equations (4)–(8):

$$x_i(t+1) = x_i(t) + \alpha \times k \times x_i(t-1) + b \times \Delta x \quad (4)$$

$$x_i(t+1) = x_i(t) + tan(\theta) \times |x_i(t) - x_i(t-1)| \quad (5)$$

$$x_i(t+1) = X^* + b_1 \times (x_i(t) - Lb^*) + b_2 \times (B_i(t) - Ub^*) \quad (6)$$

$$x_i(t+1) = x_i(t) + C_1 \times \left(x_i(t) - Lb^b\right) + C_2 \times \left(x_i(t) - Ub^b\right) \quad (7)$$

$$x_i(t+1) = X^b + S \times g \times \left(\left|x_i(t) - X^*\right| + \left|x_i(t) - X^b\right|\right) \quad (8)$$

where α is the perturbation factor, set to -1 or 1 based on a probability method; t is the current iteration count; Δx denotes the simulated light intensity change; k is the rolling direction coefficient, set to 0.1 according to the original DBO algorithm standard configuration; b is a constant set to 0.3 following benchmark settings from pioneering research; θ is the deflection angle ($\epsilon[0, \pi]$), defining the full-angle search space for the dancing behavior; Lb and Ub are the lower and upper bounds of the spawning zone, respectively; Lb^b and Ub^b denote the upper and lower bounds of the optimal foraging zone (these boundaries are not arbitrarily set but strictly mapped to the minimum/maximum permissible values of the six layout parameters defined in Table 3, ensuring optimization remains within the physically feasible design space); $Xi(t)$ represents the position information of the i-th predator beetle at iteration t; C_1 is a normally distributed random number; C_2 is a random vector with values in $\epsilon[0, 1]$; S is a constant value; g is a $1 \times D$ random vector following a normal distribution. The core algorithm parameters were directly adopted from the original DBO scheme proposed by Xue and Shen [41], which has been empirically validated to effectively balance exploration and exploitation across various optimization problems.

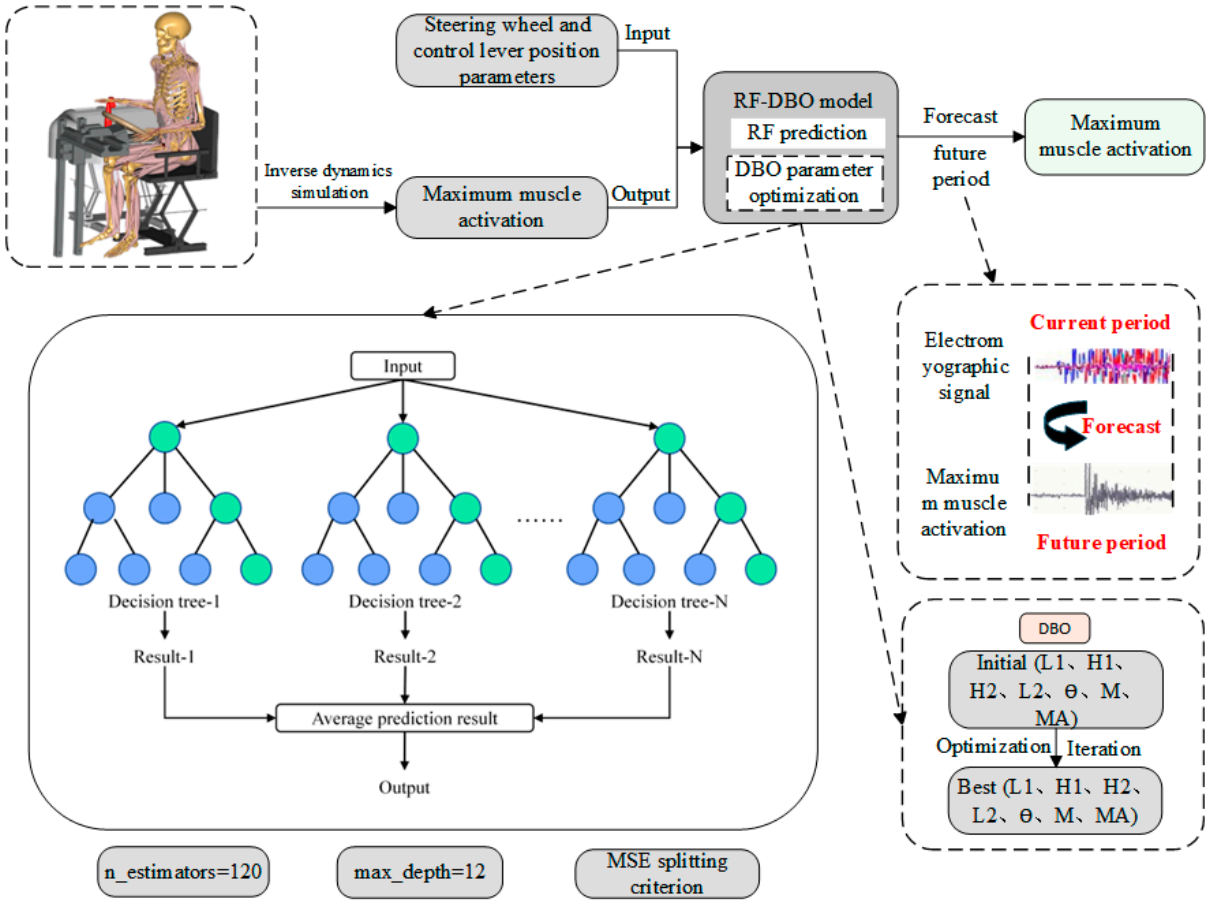


Figure 8. AMS-RF-DBO Framework.

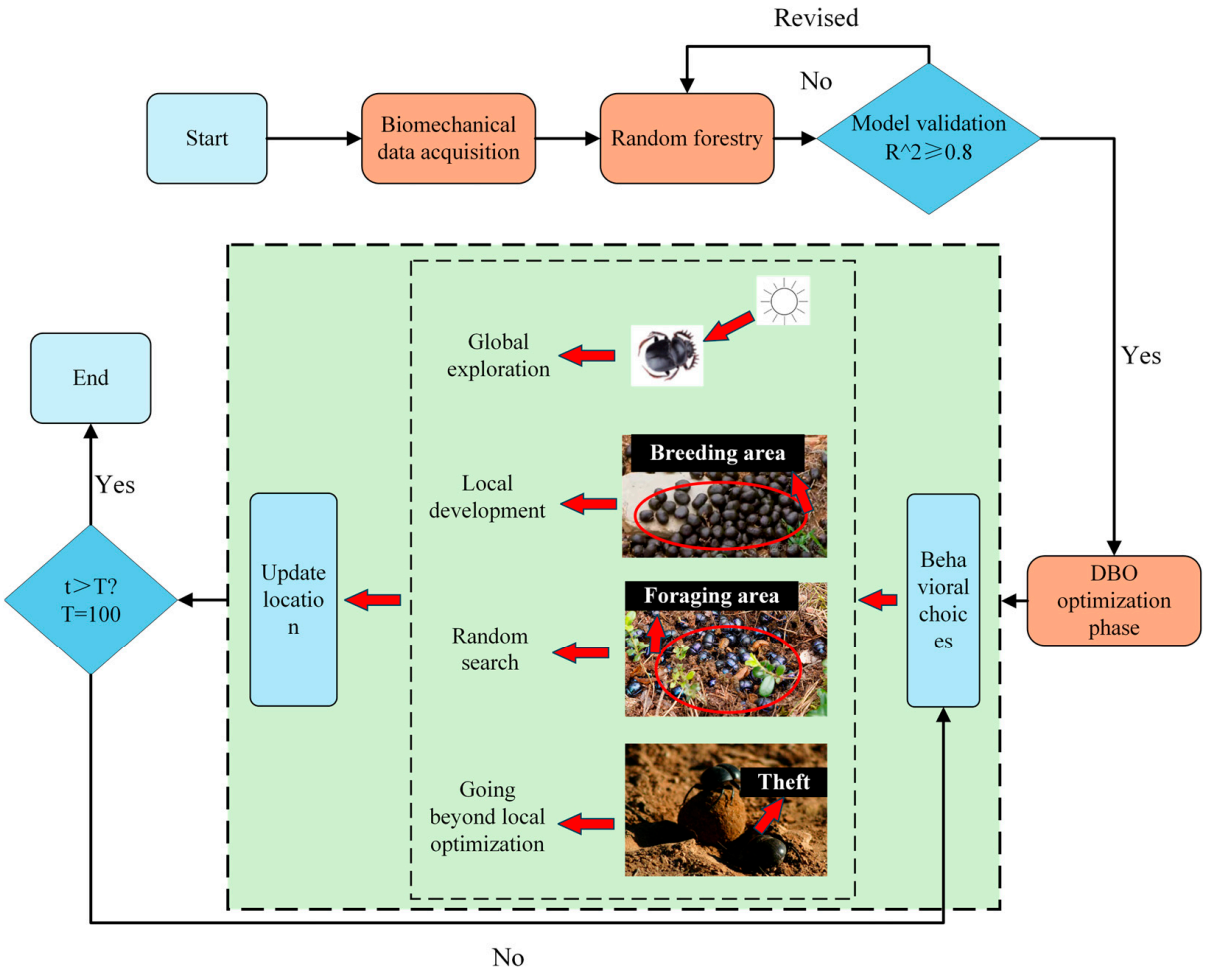


Figure 9. Flowchart of the DBO Algorithm.

3. Results

3.1. Selection of Target Muscles for sEMG Analysis

Given the unique operational requirements of cotton picker operations, biomechanical analysis of driving posture necessitates independent assessment of both upper limbs. As shown in Figure 10a, a variance analysis of changes in MA levels of the left upper-limb during the action cycle revealed a significant main effect of different muscles on MA levels (Welch's F (3, 8.53) = 46.72, $p < 0.001$, $\omega^2 = 0.82$). Post hoc tests indicated that the activation level of the lateral head of the triceps brachii was significantly lower than that of the flexor carpi radialis (MD = −1.95%, 95% CI [−2.53, −1.37]), with this difference being statistically significant ($p < 0.001$) and having a very large effect size (Cohen's d = 5.21). Meanwhile, the MA levels of the biceps brachii (MD = −1.68%, $p < 0.001$) and deltoid (MD = −2.08%, $p < 0.001$) were also significantly higher than those of the lateral head of the triceps brachii. When rotating clockwise by 90°, the MA levels of the radial wrist flexor and the middle bundle of the deltoid muscle increased to 3.47% and 2.98%, respectively. Upon rotating counterclockwise by 180°, the middle bundle of the deltoid muscle gradually entered a low-activation state, with the MA level reaching 1.05%. At the same time, the MA level of the radial wrist flexor showed a trend of first decreasing to 2.67% and then increasing to 3.71%. As the steering wheel rotated clockwise by another 90°, the radial wrist flexor and the middle portion of the deltoid muscle showed decreasing and increasing trends, respectively, ultimately approaching the MA levels at the initial position. The biceps brachii exhibited a "W"-shaped biphasic fluctuation throughout the entire movement cycle, while the MA level of the lateral head of the triceps brachii showed irregular changes. Therefore,

based on their dynamic involvement and functional contributions in driving tasks, the radial wrist flexor, biceps brachii, and middle bundle of the deltoid muscle were chosen as analytical factors for the left upper-limb muscle group, offering higher representativeness and research value.

As shown in Figure 10b, since the right hand does not involve active wrist movement during the operation, the activation of the radial wrist flexor was not included in the initial selection range. Analysis of variance (ANOVA) revealed that the MA level of the triceps brachii was significantly lower than that of the deltoid (MD = −2.17%, $p < 0.001$, d = 48.2) and the biceps brachii (MD = −2.00%, $p < 0.001$, d = 25.0). The difference between the biceps brachii and the deltoid muscle was smaller but still statistically significant (MD = −0.17%, $p = 0.021$, d = 1.7), with both muscles exhibiting activation levels greater than 1.8% and showing steady trends of change. Based on the above analysis, the biceps brachii and middle head of the deltoid muscle demonstrated higher involvement in maintaining right upper-limb postural stability and functionality. Therefore, selecting these two muscles as analytical factors for the right upper-limb muscle group holds higher scientific rationality and research value.

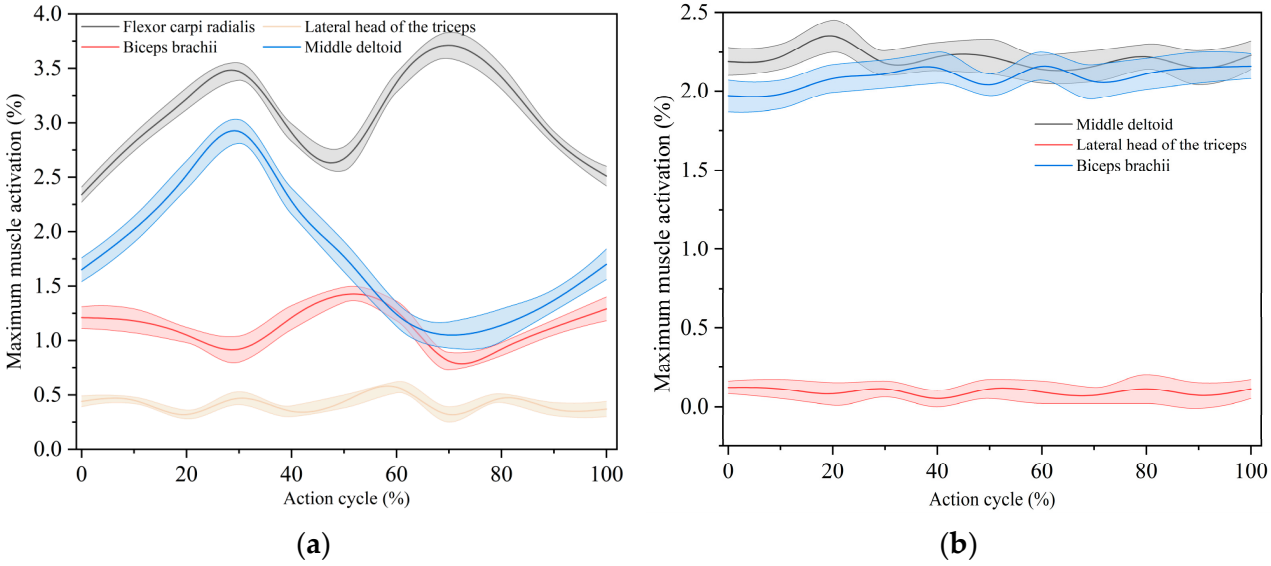


Figure 10. Schematic diagram of upper-limb muscles (The shaded area represents the standard error.): (**a**) left upper-limb and (**b**) right upper-limb.

3.2. Validation Analysis of the Biomechanical Model

As shown in Figure 11, the simulated muscle force data of the biceps brachii obtained through the AMS exhibit high agreement between predicted and experimentally measured values throughout one movement cycle when compared with the normalized linear envelope of sEMG data. However, deviations were observed at the 25% and 70% stages of the movement cycle, where the amplitude of the electromyographic signal was approximately 20% higher than the simulated values. This discrepancy may stem from simplified treatment of tendon unit stiffness parameters in the AnyBody model, as well as displacement artifacts generated by surface electrodes during high-intensity muscle contractions. Intraclass correlation coefficient analysis (ICC = 0.695, 95% confidence interval) indicated that overall consistency reached the level of strong agreement (ICC 0.6–0.8) according to the evaluation criteria established by Koo et al. [42], validating the reliability of the biomechanical model in characterizing sEMG signals.

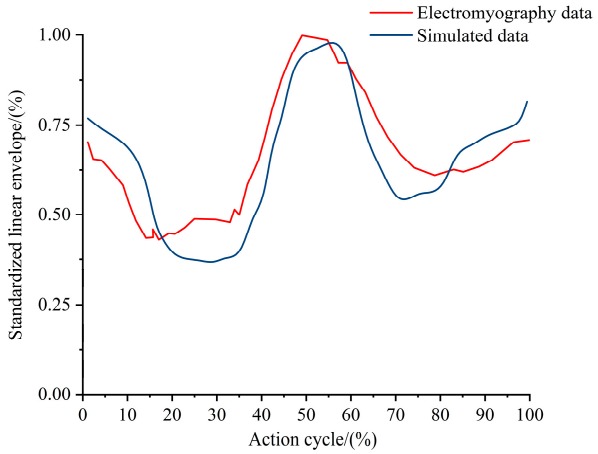


Figure 11. Comparison between the simulated muscle force from the AnyBody model and the normalized experimental sEMG linear envelope for the biceps brachii during one motion cycle.

3.3. RF Prediction Model Analysis

3.3.1. Analysis of Feature Importance

As shown in Figure 12, the SHAP [43] method was employed to quantify the contribution of each parameter to the output of the prediction model. The results show that the SHAP values for L1 have the widest distribution range, while the other parameters have relatively uniform distributions, with significant intra-group differences ($p < 0.05$). In the polar plot, this is manifested as the largest sector area and the deepest color feature, indicating that it has the most significant impact on the model output. The H1 and L2 parameters follow, showing moderate levels of contribution. In contrast, the SHAP value distributions for H2, M, and θ were the most concentrated, with relatively lower contributions. Further analysis revealed that the model outputs exhibited a distinct left–right asymmetry. Among these, the steering wheel layout parameters (particularly the distance between the steering wheel and the H-point, represented by L1) have the most prominent impact on the model output. In comparison, the overall contribution of the control stick layout parameters (L2, θ, M, H2) was relatively small, with only L2 exhibiting a moderate influence. The parameters are ranked by their contribution from highest to lowest as follows: L1 > H1 > L2 > θ > M > H2.

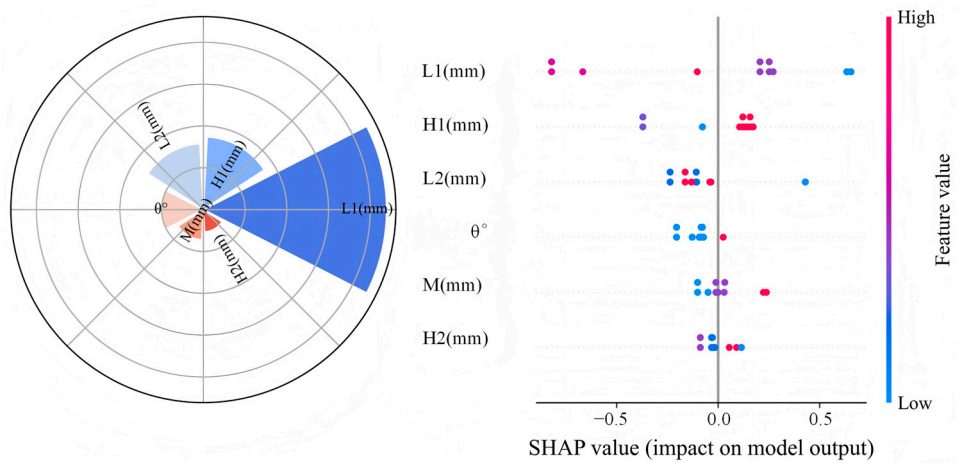
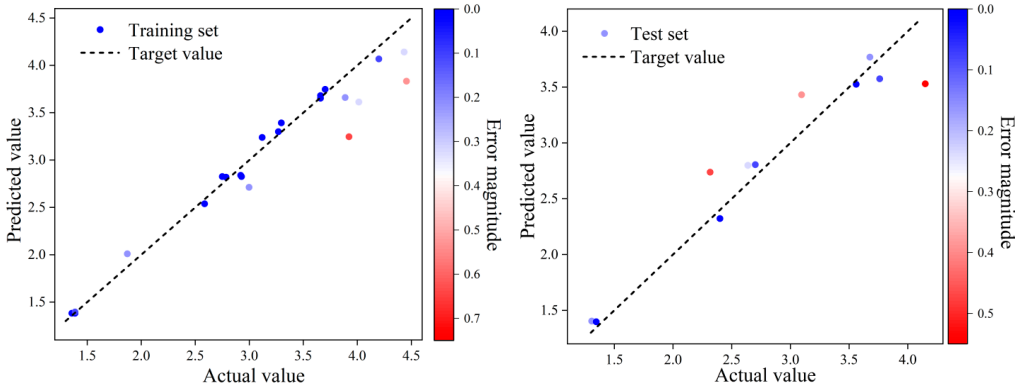


Figure 12. SHAP summary plot (**left**) and polar coordinate plot (**right**) for feature importance analysis.

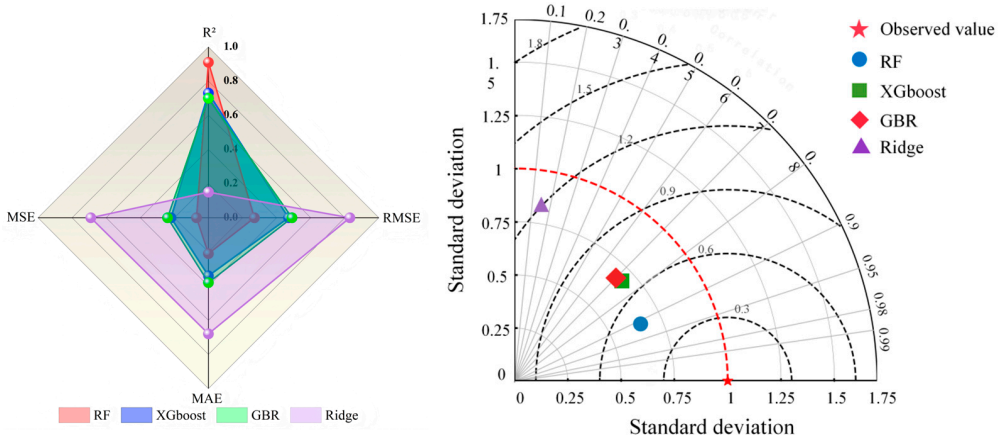
3.3.2. Comparative Analysis of RF Prediction Performance

Figure 13 presents a scatter plot of the prediction performance of the RF model on both the training and test sets. The RF model demonstrated excellent generalization ability, with a performance difference of only 1.1% between the training set (R^2 = 0.92) and the test set (R^2 = 0.91), and small differences in key error metrics (RMSE and MSE differences are less than 0.01, and MAE difference is equal to 0.03). To further evaluate the model's performance, radar charts and Taylor plots (Figure 14) were employed for a multidimensional comparative analysis. This analysis compared RF model's performance on the test set against three other models with differing optimization strategies: Extreme Gradient Boosting (XGBoost) [44], Gradient Boosting Regression (GBR) [45], and Ridge Regression (Ridge) [46]. The RF model demonstrated a significant advantage on the test set: its R2 value was 0.18, 0.21, and 0.76 higher than XGBoost, GBR, and Ridge, respectively. Additionally, the RF model outperformed the other models in terms of error metrics, including RMSE, MAE, and MSE, which were lower than those of the other three models. This confirms that the RF model provides the best overall performance in terms of prediction accuracy, robustness, and explanatory power for maximum MA levels.



(**a**) (**b**)

Figure 13. Scatter plots of predicted vs. actual MA for the (**a**) training set and (**b**) test set of the RF model.



(**a**) (**b**)

Figure 14. (**a**) Radar chart comparing model evaluation metrics. (**b**) Taylor diagram for model performance comparison.

3.4. Optimization Results Using the DBO Algorithm

This study employed a bio-inspired optimization mechanism based on DBO, simulating the foraging path planning and navigation behavior characteristics of dung beetle

populations. This mechanism establishes a multi-objective parameter optimization framework tailored to RF regression models. As shown in Figure 15, the objective function value converged to an optimal value after 100 iterations, yielding a minimum MA of 1.47% (95% CI: 1.35–1.59%, SD = 0.061%). The optimal ergonomic parameter combination was as follows: L1 = 434 mm, H1 = 738 mm, θ = 32°, L2 = 357 mm, H2 = 782 mm, and M = 411 mm. The optimized joystick position (L2 = 357 mm, H2 = 782 mm), compared with the "center point of the optimal hand operating zone in a seated position" (360 mm, 785 mm), showed a deviation of less than 1.5%, indicating no significant difference ($t(2) = -0.01$, $p = 0.992$, 95% CI [−625.6, 619.6]). This demonstrates that the optimized results possess good stability and universality. The CV of the MA value was 4.15%. The stability of the optimization results was further assessed using bootstrap resampling (n = 1000 times, σ = 0.1%). According to the process capability index mentioned in ISO 22514-4:2016 [47] (Cp = 1.67, Cpk = 1.52), the results meet the six-sigma standard for industrial applications (Cp ≥ 1.5, Cpk ≥ 1.33). This confirms that the results are reliable and can provide a certain reference for cotton picker cab layout design.

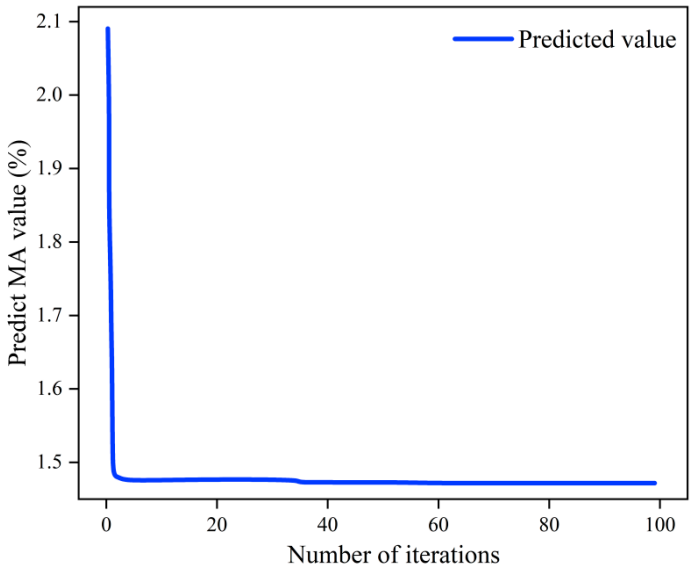


Figure 15. Convergence curve of the DBO algorithm.

Robustness Analysis of DBO Optimal Solutions

(1) The DBO algorithm was independently executed 30 times from random initializations under the identical setup. The statistical summary of the final objective function values (minimum MA) was as follows: mean = 1.48%, standard deviation (SD) = 0.018%, and 95% confidence interval = [1.473%, 1.487%]. The negligible SD and tight confidence interval demonstrate the algorithm's highly stable convergence and its insensitivity to initial conditions, effectively mitigating the risk of becoming trapped in suboptimal local minima.

(2) To assess the sensitivity of the optimal layout parameters to the inherent variability in the training data, a bootstrap resampling procedure with 1000 iterations was performed. In each iteration, a new training dataset was created by random sampling with replacement from the original dataset, a new RF surrogate model was trained, and the DBO optimization was executed anew. The 95% confidence intervals (CIs) for the six optimized parameters, derived from the bootstrap distribution, are summarized in Table 5.

Table 5. Bootstrap analysis of optimal layout parameters (n = 1000 resamples).

Parameter	Optimal Value	95% CI Lower Bound	95% CI Upper Bound	CI Width	Relative Width (% of Optimal)
L1 (mm)	434	429	439	10	2.3%
H1 (mm)	738	733	743	10	1.4%
θ (°)	32	30.5	33.5	3.0	9.4%
L2 (mm)	357	354	360	6	1.7%
H2 (mm)	782	779	785	6	0.8%
M (mm)	411	408	414	6	1.5%

The results indicate that the confidence intervals for all parameters are relatively narrow, with absolute widths $\leq$ 10 mm (3.0° for the θ parameter) and relative widths (confidence interval width/optimal value) all below 10%, with most falling below 2%. This demonstrates that the optimal solution exhibits statistically significant robustness to perturbations in the training data.

(3) During training, the RF model automatically identifies and filters out random fluctuations and incidental errors in the raw electromyography data, thereby constructing a predictive model that reflects the true, stable relationship between parameters and muscle load. DBO performs computations and optimization directly on this predictive model. This means the optimization algorithm consistently "perceives" a clear, reliable target landscape rather than the noisy raw data surface. Consequently, from data input to output results, noise impacts are effectively buffered and isolated within the framework, significantly enhancing the reliability of the optimization solution.

4. Discussion

In the field of agricultural engineering, previous research has primarily focused on optimizing the cab layout of traditional agricultural machinery such as tractors, with particular emphasis on the ergonomic adaptation of seats, steering wheels, and control levers. However, research on optimizing the cab layout for specialized agricultural machinery like cotton pickers remains insufficient. Given the high operational intensity, concentrated working hours, and harsh environmental conditions associated with cotton picking, scientifically optimizing the cab layout to enhance operator comfort has become a critical issue requiring urgent attention. This study proposes an innovative AMS-RF-DBO framework that integrates sEMG signals with inverse dynamics analysis to evaluate how different layout parameters affect upper-limb MA levels. Based on this analysis, the DBO optimization algorithm is employed to refine the cab layout parameters, identifying the optimal configuration that minimizes MA levels, thereby enhancing operational comfort and efficiency. The findings reveal that the optimized layout parameters significantly reduces upper-limb muscle load, filling a critical gap in the ergonomic design of specialized agricultural machinery.

4.1. Upper-Limb MA Patterns

This study analyzed the activation characteristics of upper-limb muscles in drivers to reveal the functional differentiation and cooperative mechanisms of different muscle groups during driving tasks. To visually demonstrate the consistency of muscle activation patterns across subjects, real-time surface electromyography waveforms of the radial wrist flexors during driving tasks for 10 participants were compiled and presented in Appendix A. The results indicated that under standard driving postures, the activation level of the left upper-limb biceps brachii was relatively low and did not change significantly over time, which may be related to its lower functional requirements during driving. Due to the

elbow joint maintaining a micro-flexion state for an extended period, the active contraction demand for the biceps brachii as an elbow flexor decreases, resulting in a smaller flexion torque, which is partially offset by the tension of passive structures such as the elbow joint capsule and ligaments. This finding aligns with the "energy minimization" principle of muscle coordination [48]. At this point, the biceps brachii, as an active flexor, only needs to provide minimal compensatory contraction force, thus maintaining its electromyographic activity at a low level. This finding is consistent with previous studies, which indicate that MA levels are closely related to joint movement requirements in static postures [49].

In contrast, the activation trends of the radial wrist flexor, biceps brachii, and middle deltoid were more pronounced, indicating that these muscles play more important functional roles during driving.

(1) Biceps brachii: When gripping the steering wheel, the elbow joint typically remains flexed at 90–120°. The biceps brachii, as part of the primary elbow flexor muscle group (working in conjunction with the brachialis and brachioradialis muscles), must maintain continuous isometric contraction to counteract gravity and prevent the arm from drooping. In the steering wheel grip position, the lever arm of the biceps brachii (the vertical distance from the elbow joint rotation center to the tendon insertion point) enables it to efficiently maintain torque balance. Throughout the entire movement cycle, the "W"-shaped fluctuation of the biceps brachii is essentially the result of the combined effects of pronation/supination torque demands and the transition between eccentric and concentric contractions, reflecting its dynamic adaptation to multi-directional rotational loads.
(2) Flexor carpi radialis: As one of the primary wrist flexors, the flexor carpi radialis is responsible for wrist flexion and radial deviation (toward the thumb side), which aligns closely with wrist movements during steering wheel control. However, MA is not prominent in the static driving posture of the right hand, a conclusion consistent with the findings of Mark et al., who reported that the sEMG amplitude of the radial wrist flexor is greater during dynamic steering than during static grip [50].
(3) Middle deltoid: The middle deltoid muscle, as the primary muscle group responsible for shoulder abduction, sustains activation to counteract gravitational forces, thereby ensuring upper-limb stability in the horizontal plane. This function aligns closely with the biomechanical demands of the suspended arm posture during driving. The maximum level of MA throughout the action cycle exhibits an "ascending–descending–ascending" pattern, reflecting adaptive regulation during dynamic rotation—from active force generation (concentric) to synergistic control (eccentric) and finally to active compensation (antigravity/deceleration). Its activation level remains positively correlated with the shoulder joint abduction torque demand.

For the right upper-limb, activation of the middle bundle of the deltoid muscle was relatively high, further confirming its central role in maintaining shoulder joint stability. In contrast, the activation level of the lateral head of the triceps brachii was relatively low, possibly because the elbow joint was in a neutral position when the right hand was fixed on the control handle, reducing the need for elbow flexion. This phenomenon suggests that, in static driving postures, MA patterns are more dependent on the mechanical state of the joint than on active movement requirements.

The muscle combinations selected in this study (left upper-limb: flexor carpi radialis, lateral head of the triceps brachii, and middle bundle of the deltoid muscle; right upper-limb: middle bundle of the deltoid muscle and biceps brachii) not only reflect dynamic participation characteristics of different muscle groups during driving tasks but also provide a theoretical basis for future driving posture optimization and human–machine interaction design. For example, adjusting steering wheel resistance or seat armrest height can reduce

fatigue risks for postural muscle groups such as the deltoid muscle. These findings not only validate the established muscle model but also elucidate the close relationship between MA and joint biomechanical demands during driving. They provide a theoretical basis for optimizing the human–machine interaction design of cotton picker cab control layouts to reduce upper-limb muscle fatigue and mitigate the risk of WMSDs.

4.2. AMS-RF-DBO Framework Validation and Optimization

Compared with traditional human factors optimization methods, the AMS-RF-DBO framework proposed in this study demonstrates significant advantages across multiple aspects. First, the framework achieves deep integration of high-fidelity biomechanical simulation and data-driven intelligent optimization. Conventional approaches predominantly rely on generic digital human models or limited sEMG experimental data, which struggle to accurately capture individual muscle load responses under specific dynamic working postures. By constructing a driver–cabin coupled biomechanical model through AMS, our framework provides MA data with high physiological fidelity based on first-principles inverse dynamics calculations. The large-scale dataset generated by this model is used to train an RF regression model, thereby establishing a computationally efficient surrogate model that accurately predicts MA levels under different layout parameters. This effectively overcomes the limitations of relying solely on experiments (high cost abd limited sample size) or pure simulation.

Second, the framework incorporates an intelligent optimization algorithm that effectively avoids local optima when handling multi-parameter optimization problems, thereby reliably identifying global or near-global optimal solutions that minimize MA levels. Although this research focuses on the cab layout of cotton pickers, the core methodology of AMS-RF-DBO can be transferred to human factors design for other types of specialized agricultural machinery, construction equipment, or industrial cabins. By replacing the corresponding biomechanical models and design variables, the framework can provide a systematic technical pathway for improving operational comfort across different working scenarios.

As a specific validation case of the proposed AMS-RF-DBO framework, this study applied the framework to optimize cotton picker cab layout. To reduce upper-limb muscle fatigue in cotton picker drivers during operations, this study constructed an RF prediction model using three key position parameters for the steering wheel and control lever as inputs and MA as the output. The RF model demonstrated high predictive accuracy ($R^2 = 0.927$) and could reliably estimate MA values under different position parameters. After applying the DBO algorithm, an efficient parameter space search was achieved, converging to the optimal solution after 100 iterations. The optimized steering wheel layout parameters in this study are highly consistent with the optimal configuration of tractor steering wheels reported by Xu et al., with average relative errors of 3.17%, 0.69%, and 6.33% for θ, L1, and H1, respectively. The slightly larger deviation of H1 may be attributed to the unique two-handed operation mode of the cotton picker and differences in driving visibility compared to tractors. A key advantage of this study is that it explicitly considers the interactions during right-hand control lever operation, an aspect not addressed in previous studies. The DBO optimization algorithm reached a stable state after 87 iterations, demonstrating good exploration–exploitation balance. Parameter optimization reduced the comprehensive MA of upper-limb muscles from 3.82% to 1.47%, indicating a 61.5% reduction in peak muscle load, which is of significant importance for prolonged cotton sspicking operations. This aligns with the findings of GENC et al. [51], who identified a significant relationship between MA and peak muscle load ($p < 0.001$). The optimized parameters minimized the sustained contraction intensity of the middle deltoid muscle and radial wrist flexor, which

are the muscle groups most prone to fatigue during repetitive turning operations [52]. The significant reduction in muscle load achieved in this cotton picker case study effectively validates the practical efficacy and reliability of the proposed AMS-RF-DBO framework.

4.3. Consideration of Model Assumptions

The level of MA fundamentally depends on the muscle recruitment criteria employed within the AMS inverse dynamics solver. While the adopted "minimum/maximum" stress criterion represents a physiologically driven and widely used assumption, alternative criteria—such as minimizing linear stress or square stress—may yield absolute differences in force distribution among synergistic muscle groups. Nevertheless, the core comparative objective of this study—identifying cockpit layouts that minimize upper-limb MA relative to a baseline configuration—remains unaffected by this choice. This is because the relative ranking and trends of MA across different layout designs are preserved when all simulations employ the same consistent recruitment criterion. Future research aiming to establish absolute muscle load thresholds for safety standards would benefit from incorporating sensitivity analyses that evaluate different recruitment strategies.

4.4. Limitations and Future Perspectives

Although this study provides an effective solution for optimizing upper-limb muscle fatigue for cotton picker operators, several limitations remain. First, the sample size was relatively small (n = 10), and the participant group had a homogeneous age structure. While it covered the human body size range specified in the 50th percentile of the GB/T 10000-2023 standard, it did not adequately account for gender differences or the needs of operators with special body types, which may affect the generalizability of the study's conclusions. Second, the experimental scenario only simulated straight-line harvesting operations and did not cover all actual operational conditions, such as turning at field edges or reversing maneuvers. Additionally, the current study was conducted under laboratory simulation conditions and did not fully replicate the effects of vibration spectra and complex terrain on muscle load during real-world vehicle operations. Future research recommendations are as follows: (1) Regarding the subject population, the sample size was relatively small (n = 10) and homogeneous in terms of age and anthropometric characteristics (50th percentile for Chinese males). While the optimized layout parameters demonstrated significant effectiveness for the target population represented by this sample, further validation is required to directly extrapolate these findings to broader, more heterogeneous populations (e.g., different percentiles, female, or elderly operators). Future research should prioritize recruiting larger and more diverse samples (>30 participants) encompassing different percentiles, genders, and age groups to validate the framework's universality and establish population-adjusted design guidelines. (2) The experimental scenario in this study simulated only straight-line operations. Actual cotton harvesting involves complex multi-directional tasks that impose fundamentally different biomechanical demands compared to the continuous, primarily sagittal-plane forces experienced during straight-line travel. Future research could address this gap by developing multi-scenario experimental protocols incorporating steering and complex maneuvers. (3) Conduct real vehicle testing and simultaneously collect whole-body electromyography signals. (4) Develop a whole-body ergonomics optimization algorithm based on multi-body dynamics modeling, with a focus on assessing biomechanical loads on the lumbar spine and knee joints. (5) This study lacks explicit fatigue analysis for prolonged work sessions. The optimization scheme relies on instantaneous peak MA, a metric reflecting short-term load but fails to capture fatigue progression over time—a critical factor in repetitive agricultural tasks. While the optimized layout reduces immediate muscular demands, its effectiveness in delaying fatigue onset or

sustaining comfort during extended work remains to be validated. Future research should incorporate long-term testing and fatigue-sensitive sEMG metrics to evaluate and optimize sustained ergonomic performance. (6) This study relies solely on sEMG to infer comfort or ergonomic suitability. However, surface electromyography lacks persuasiveness due to its susceptibility to electrode placement, signal crosstalk, and non-fatigue factors. Future research may integrate subjective ratings, force metrics, or joint torque measurements for a more comprehensive evaluation.

5. Conclusions

This study effectively tackles the critical ergonomic issue of upper-limb WMSDs among cotton picker operators caused by unsuitable cab layouts. A reproducible AMS-RF-DBO framework was developed and validated to enhance operator comfort and support sustainable mechanized cotton harvesting. The framework also shows strong potential for ergonomic design in other specialized agricultural and industrial vehicles. The key conclusions are as follows:

(1) A high-fidelity driver–cabin biomechanical model was established using the AnyBody Modeling System. Critically, its validation against experimental sEMG data (ICC = 0.695) confirms that the model can reliably replicate the unique neuromuscular demands of the "left-hand steering, right-hand lever" operation in the participant sample. This step successfully translated a complex real-world ergonomic scenario into a computable and analyzable digital framework, providing a physiologically credible basis for all subsequent analyses, rather than just a simulation output.

(2) A Random Forest regression model was constructed using six key cab layout parameters as inputs. Its high predictive accuracy (R^2 = 0.91) demonstrates a successful abstraction—it effectively learned the underlying, nonlinear relationship between spatial design and physiological load from the dataset generated by the biomechanical model. This success means that for the represented operator population, muscle activation can be accurately forecasted without repetitive, costly simulations, fundamentally streamlining the ergonomic evaluation process and enabling rapid design exploration.

(3) Through the DBO optimization algorithm, the MA level of the upper limbs of cotton picker drivers was minimized, and the optimal parameter combination was obtained as L1 = 434 mm, H1 = 738 mm, θ = 32°, L2 = 357 mm, H2 = 782 mm, M = 411 mm, H2 = 782 mm, and θ = 32°. The MA value significantly decreased from the initial 3.82% to 1.47% ($p < 0.001$), with a 61.5% reduction in peak muscle load. The study results provide a new method for the ergonomic design of cotton picker cabs in China, offering technical support for improving operator comfort.

Author Contributions: H.T.: Writing—Original Draft, Visualization, Software, Methodology, Investigation, Formal Analysis, Conceptualization, and Data Curation. Z.W.: Software, Methodology, Investigation, Conceptualization, and Funding Acquisition. Y.Z.: Supervision, Resources, Project Administration, and Funding Acquisition. Y.L.: Writing—Review and Editing, Visualization, Investigation, Conceptualization, and Data Curation. Z.H. Writing—Review and Editing, Visualization, Investigation, Conceptualization, and Data Curation. J.G.: Writing—Review and Editing, Visualization, Investigation, and Conceptualization. Y.W.: Writing—Review and Editing, Visualization, Investigation, and Conceptualization. All authors have read and agreed to the published version of the manuscript.

Funding: This research was supported by the Science and Technology Program of Xinjiang Production and Construction Corps (Award No: 2023ZD058).

Institutional Review Board Statement: This study was conducted in accordance with the principles of the Declaration of Helsinki and was approved by the Ethics Committee of the First Affiliated Hospital of Shihezi University (Approval No. [KJ2025-393-02]. Date of approval: [4 September 2025]).

Informed Consent Statement: Informed consent was obtained from all participants.

Data Availability Statement: The original contributions presented in this study are included in the article. Further inquiries can be directed to the corresponding authors.

Acknowledgments: The authors sincerely thank Hengzhi Technology for providing the experimental instruments and equipment.

Conflicts of Interest: The authors declare that they have no known competing financial interests or personal relationships that could have appeared to influence the work reported in this paper.

Appendix A

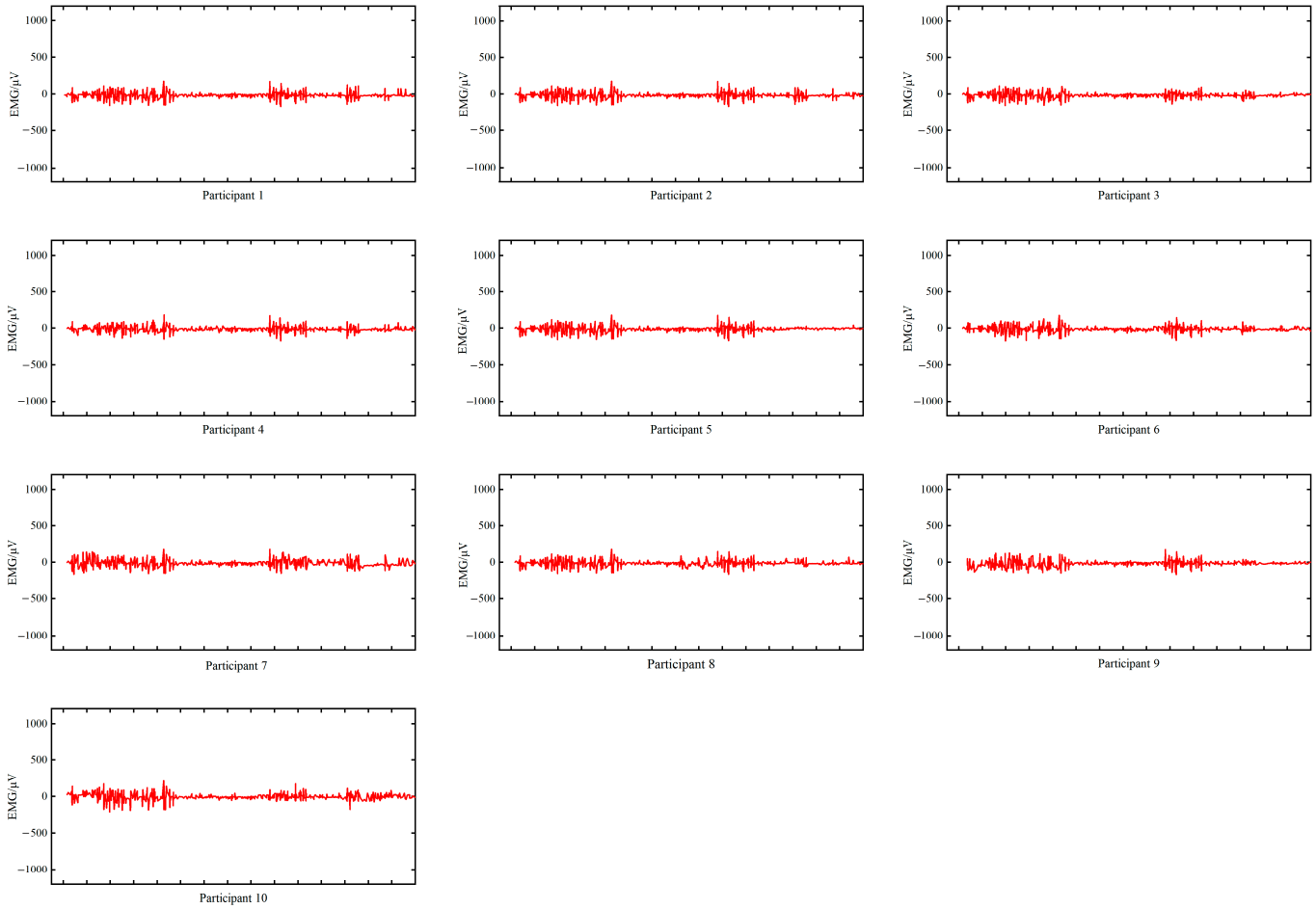


Figure A1. EMG waveform comparison of the left flexor carpi radialis across 10 participants.

References

1. Tian, L.; Lou, S.; Zhang, P.; Du, M.; Luo, H.; Li, J.; Parhat, M.; Ma, T.; Zhang, L. Analysis of Challenges and Solutions for Increasing Cotton Yields in Xinjiang Under Green and Efficient Production Models. *Chin. J. Agric. Sci.* **2025**, *58*, 1102–1115.
2. Ni, G.; Li, B.; Liu, Y.; Li, Y.; Wang, T.; Wang, S. The Development History and Current Research Status of Cotton Pickers in China. *Chin. J. Agric. Mach. Chem.* **2020**, *41*, 212–218. [CrossRef]
3. Baikeli, Y.; Zhang, J.; Guo, G.; Mahemet, A. Review and Development Trends of Mechanized Cotton Stalk Harvesting Technology in Xinjiang Cotton-Growing Regions. *Agric. Mech. Res.* **2025**, *47*, 292–300. [CrossRef]
4. Madaleno, P.; Sousa-Uva, A. Occupational Risk Perception and Occupational and Work-Related Diseases Prevention. *Eur. J. Public Health* **2021**, *31*, ckab165.436. [CrossRef]

5. Wang, J.; Zhang, Z.; Zhang, N.; Liang, Y.; Gong, Z.; Wang, J.; Ditta, A.; Sang, Z.; Li, X.; Zheng, J. The Correlation of Machine-Picked Cotton Defoliant in Different Gossypium Hirsutum Varieties. *Agronomy* **2023**, *13*, 2151. [CrossRef]
6. Gómez-Galán, M.; González-Parra, J.-M.; Pérez-Alonso, J.; Golasi, I.; Callejón-Ferre, Á.-J. Forced Postures in Courgette Greenhouse Workers. *Agronomy* **2019**, *9*, 253. [CrossRef]
7. Leder Horina, J.; Blašković Zavada, J.; Slavulj, M.; Budimir, D. Ergonomics Study of Musculoskeletal Disorders among Tram Drivers. *Appl. Sci.* **2025**, *15*, 8348. [CrossRef]
8. Ortiz, E.; Baño-Morales, D.; Venegas, W.; Page, Á.; Guerra, S.; Narváez, M.; Zambrano, I. Evaluation of Technical and Anthropometric Factors in Postures and Muscle Activation of Heavy-Truck Vehicle Drivers: Implications for the Design of Ergonomic Cabins. *Appl. Sci.* **2025**, *15*, 7775. [CrossRef]
9. Burgess-Limerick, R. Participatory Ergonomics: Evidence and Implementation Lessons. *Appl. Ergon.* **2018**, *68*, 289–293. [CrossRef]
10. Fethke, N.B.; Schall, M.C.; Merlino, L.A.; Chen, H.; Branch, C.A.; Ramaswamy, M. Whole-Body Vibration and Trunk Posture during Operation of Agricultural Machinery. *Ann. Work Expo. Health* **2018**, *62*, 1123–1133. [CrossRef]
11. Benos, L.; Tsaopoulos, D.; Bochtis, D. A Review on Ergonomics in Agriculture. Part II: Mechanized Operations. *Appl. Sci.* **2020**, *10*, 3484. [CrossRef]
12. Mansfeld, A.; Luebke, A.; Duffy, V.G. Review and Assessment of Excavator Operations Using RAMSIS Ergonomic Engineering Software. In *HCI International 2022—Late Breaking Papers: Ergonomics and Product Design*; Duffy, V.G., Rau, P.-L.P., Eds.; Lecture Notes in Computer Science; Springer Nature: Cham, Switzerland, 2022; Volume 13522, pp. 275–295, ISBN 978-3-031-21703-6.
13. Wu, Y.; Zhou, Z.; Xi, Z.; Li, J. Tractor Cab Virtual Modeling and Ergonomic Evaluation Based on Jack. In Proceedings of the ASME International Design Engineering Technical Conferences and Computers and Information in Engineering Conference, 2018, Quebec City, QC, Canada, 26–29 August 2018; American Society of Mechanical Engineers: New York, NY, USA, 2018; Volume 3, p. V003T01A016.
14. Wang, S.; Liang, J.; Shi, Y. Ergonomic Analysis and Improvement Design of the Jack-Based Mining Loader Cabin. *J. Mech. Des.* **2024**, *41*, 170–176. [CrossRef]
15. Wang, X.; Jiang, X.; Yang, G.; Ma, M.; Zhao, W.; Liu, X.; Liu, W. Research on Layout Optimization of Human-Machine Interface for Laser Additive Manufacturing Equipment Based on Accessible Domain. *J. Mech. Eng.* **2023**, *59*, 317–330. [CrossRef]
16. Qu, W.; Ma, L.; Xu, J.; Yang, B. Design of Evaluation System for Workover Rig Operation Posture Comfort Based on Creo. *Ind. Eng. J.* **2022**, *25*, 168–172. [CrossRef]
17. Cheng, L.; Wen, H.; Ni, X.; Zhuang, C.; Zhang, W.; Huang, H. Optimization Study on the Comfort of Human-Seat Coupling System in the Cab of Construction Machinery. *Machines* **2022**, *11*, 30. [CrossRef]
18. Rathod, A.B.; Vyavhare, R.T. Optimization of Truck Driver Cab Ergonomic for Commercial Truck Based on Ramsis: Enhancing Driver Comfort and Safety. *Int. J. Intell. Transp. Syst. Res.* **2024**, *22*, 603–613. [CrossRef]
19. Cen, C.; Cheng, S.; Wong, N.H. Physiological Sensing of Personal Thermal Comfort with Wearable Devices in Fan-Assisted Cooling Environments in the Tropics. *Build. Environ.* **2022**, *225*, 109622. [CrossRef]
20. Zhang, H.; Meng, L.; Yang, Z. Biomechanical Mechanism Driving Typical Postural Shifts of Lower Limbs during Sleeping in an Aircraft Seat. *Eur. J. Appl. Physiol.* **2023**, *123*, 2023–2039. [CrossRef]
21. Lecocq, M.; Lantoine, P.; Bougard, C.; Allègre, J.-M.; Bauvineau, L.; Bourdin, C.; Marqueste, T.; Dousset, E. Neuromuscular Fatigue Profiles Depends on Seat Feature during Long Duration Driving on a Static Simulator. *Appl. Ergon.* **2020**, *87*, 103118. [CrossRef]
22. Chi, J.Y.; Halaki, M.; Booker, E.; Boyle, R.; Ackermann, B.J. Interaction between Hand Span and Different Sizes of Keyboards on EMG Activity in Pianists: An Observational Study. *Appl. Ergon.* **2021**, *97*, 103518. [CrossRef]
23. Xin, Y.; Bai, W.; Jin, H.; Zhang, Q.; Su, N. Analysis of Upper Limb Muscle Fatigue in Excavator Operators Based on Electromyography Experiments. *Sci. Technol. Eng.* **2024**, *24*, 11393–11400.
24. Chen, D. Inverse Dynamics Simulation of the Musculoskeletal Model of Human Legs in Driving Based on AnyBody Modeling System. *Chin. J. Biomed. Eng.* **2013**, *32*, 124–128. [CrossRef]
25. Xu, H.; Wang, Q.; Zhang, W.; Yang, H.; Zhang, G. Optimization of Tractor Seat Position Parameters Based on Driver Biomechanical Characteristics. *Trans. Chin. Soc. Agric. Eng.* **2022**, *38*, 32–40.
26. Zhang, W.; Wang, Q.; Xu, Z.; Shang, Y.; Xu, H. Development of a Tractor Operator-Operation Environment Coupled Biomechanical Model and Analysis of Lower Limb Muscle Fatigue. *Int. J. Ind. Ergon.* **2023**, *93*, 103407. [CrossRef]
27. Xu, H.; Yang, H.; Shang, Y.; Zhang, Y.; Liu, Z.; Wang, Q.; Zhang, G. Optimization of the Key Position Parameters for Tractor Steering Wheel Based on a Driver's Arm Muscle Load Analysis. *Int. J. Agric. Biol. Eng.* **2023**, *16*, 236–247. [CrossRef]
28. Prakash, A.; Sarlin, P.J.; Thomas, J.A. Optimization of Conditions for Gelatin Extraction from Longtail Butterfly Ray, Gymnura Poecilura Skin Using Response Surface Methodology (RSM). *Food Anal. Methods* **2025**, *18*, 2672–2687. [CrossRef]
29. Zhang, W.; Yang, H.; Li, Y.; Zhao, Y.; Xu, H. An Optimization Model of Tractor Clutch Pedal Design Parameters Based on Lower Limb Biomechanical Characteristics. *Int. J. Ind. Ergon.* **2023**, *98*, 103519. [CrossRef]

30. Xie, Y.; Liu, C.; Li, W.; Du, M.; Feng, K. Optimization of Stamping Process Parameters Based on an Improved Particle Swarm Optimization–Genetic Algorithm and Sparse Auto-Encoder–Back-Propagation Neural Network Model. *Eng. Optim.* **2024**, *56*, 252–273. [CrossRef]
31. Bharat, N.; Bose, P.S.C. Integrating Genetic Algorithms, Particle Swarm, and Neural Networks for Wear Optimization of AA7178 Matrix with Nano-SiC Particles. *JOM* **2024**, *76*, 2772–2785. [CrossRef]
32. Damsgaard, M.; Rasmussen, J.; Christensen, S.T.; Surma, E.; De Zee, M. Analysis of Musculoskeletal Systems in the AnyBody Modeling System. *Simul. Model. Pract. Theory* **2006**, *14*, 1100–1111. [CrossRef]
33. Ashtiani, M.B.; Akhavanfar, M.; Li, L.; Kim, S.; Nussbaum, M.A. Using Musculoskeletal Models to Estimate the Effects of Exoskeletons on Spine Loads during Dynamic Lifting Tasks: Differences between OpenSim and the AnyBody Modelling System. *J. Biomech.* **2025**, *188*, 112780. [CrossRef]
34. *GB/T 10000-2023*; Human Dimensions of Chinese Adults. National Standards of the People's Republic of China: Beijing, China, 2023.
35. Leone, A.; Carluccio, A.M.; Caroppo, A.; Manni, A.; Rescio, G. A Systematic Review of Surface Electromyography in Sarcopenia: Muscles Involved, Signal Processing Techniques, Significant Features, and Artificial Intelligence Approaches. *Sensors* **2025**, *25*, 2122. [CrossRef]
36. Murphy, B.B.; Scheid, B.H.; Hendricks, Q.; Apollo, N.V.; Litt, B.; Vitale, F. Time Evolution of the Skin–Electrode Interface Impedance under Different Skin Treatments. *Sensors* **2021**, *21*, 5210. [CrossRef] [PubMed]
37. Al-Ayyad, M.; Owida, H.A.; De Fazio, R.; Al-Naami, B.; Visconti, P. Electromyography Monitoring Systems in Rehabilitation: A Review of Clinical Applications, Wearable Devices and Signal Acquisition Methodologies. *Electronics* **2023**, *12*, 1520. [CrossRef]
38. Vecchio, A.D.; Hug, F.; Merletti, R.; Farina, D. JEK-ISEK Tutorials on Electromyography and Kinesiology: A Summary and a Call for the next Series of Tutorials. *J. Electromyogr. Kinesiol.* **2025**, *81*, 102986. [CrossRef]
39. Boettcher, C.E.; Ginn, K.A.; Cathers, I. Standard Maximum Isometric Voluntary Contraction Tests for Normalizing Shoulder Muscle EMG. *J. Orthop. Res.* **2010**, *26*, 1591–1597. [CrossRef]
40. Hermens, H.J.; Freriks, B.; Disselhorst-Klug, C.; Rau, G. Development of Recommendations for SEMG Sensors and Sensor Placement Procedures. *J. Electromyogr. Kinesiol.* **2000**, *10*, 361–374. [CrossRef] [PubMed]
41. Frazao, M.; Silva, P.E.; Pereira Cacau, L.D.A.; Petrucci, T.R.; Assis, M.C.; Santos, A.D.C.; Brasileiro-Santos, M.D.S. EMG Breakpoints for Detecting Anaerobic Threshold and Respiratory Compensation Point in Recovered COVID-19 Patients. *J. Electromyogr. Kinesiol.* **2021**, *59*, 102567. [CrossRef] [PubMed]
42. Koo, T.K.; Li, M.Y. A Guideline of Selecting and Reporting Intraclass Correlation Coefficients for Reliability Research. *J. Chiropr. Med.* **2016**, *15*, 155–163. [CrossRef]
43. Strumbelj, E.; Kononenko, I. An Efficient Explanation of Individual Classifications Using Game Theory. *J. Mach. Learn. Res.* **2010**, *11*, 1–18.
44. Chen, T.; Guestrin, C. XGBoost: A Scalable Tree Boosting System. In Proceedings of the 22nd ACM SIGKDD International Conference on Knowledge Discovery and Data Mining, San Francisco, CA, USA, 13–17 August 2016; ACM: New York, NY, USA, 2016; pp. 785–794.
45. Friedman, J.H. Greedy Function Approximation: A Gradient Boosting Machine. *Ann. Stat.* **2001**, *29*, 1189–1232. [CrossRef]
46. Hoerl, A.E.; Kennard, R.W. Ridge Regression: Biased Estimation for Nonorthogonal Problems. *Technometrics* **2000**, *42*, 80–86. [CrossRef]
47. *ISO 22514-4:2016*; Statistical Methods in Process Management—Capability and Performance—Part 4: Process Capability Estimates and Performance Measures. ISO: Geneva, Switzerland, 2016.
48. Prilutsky, B.I.; Zatsiorsky, V.M. Optimization-Based Models of Muscle Coordination. *Exerc. Sport Sci. Rev.* **2002**, *30*, 32–38. [CrossRef]
49. McGill, S.M.; Grenier, S.; Kavcic, N.; Cholewicki, J. Coordination of Muscle Activity to Assure Stability of the Lumbar Spine. *J. Electromyogr. Kinesiol.* **2003**, *13*, 353–359. [CrossRef]
50. Porter, J.M.; Gyi, D.E. Exploring the Optimum Posture for Driver Comfort. *Int. J. Veh. Des.* **1998**, *19*, 255–266. [CrossRef]
51. Genç, S.; Güdücü, Ç.; Çek, M.E.; Mancı, E.; Günay, E. The Effect of Resistance Based Post-Activation Performance Enhancement Interventions at Different Loads on Maximal Voluntary Isometric Contraction and Muscle Activation: Preliminary Findings. *Isokinet. Exerc. Sci.* **2025**, *33*, 161–170. [CrossRef]
52. Chua, M.X.; Okubo, Y.; Peng, S.; Do, T.N.; Wang, C.H.; Wu, L. Analysis of Fatigue-Induced Compensatory Movements in Bicep Curls: Gaining Insights for the Deployment of Wearable Sensors. *IEEE Trans. Med Robot. Bionics* **2024**, *6*, 1147–1157. [CrossRef]

Disclaimer/Publisher's Note: The statements, opinions and data contained in all publications are solely those of the individual author(s) and contributor(s) and not of MDPI and/or the editor(s). MDPI and/or the editor(s) disclaim responsibility for any injury to people or property resulting from any ideas, methods, instructions or products referred to in the content.